American Mineralogist, Volume 59, pages 1166–1176, 1974

The Crystal Structures of Gillespite I and II: A Structure Determination at High Pressure

ROBERT M. HAZEN, AND CHARLES W. BURNHAM

Department of Geological Sciences,[1] Harvard University, Hoffman Laboratory, Cambridge, Massachusetts 02138

Abstract

The crystal structure of gillespite I ($BaFeSi_4O_{10}$; $a = 7.5164(6)$, $c = 16.0768(10)$ Å; $Z = 4$; $P4/ncc$) has been refined at room pressure by least-squares analysis of three-dimensional X-ray diffraction data to a weighted R value of 3.3 percent. Average bond lengths are: Si-O = 1.603, Ba-O = 2.832, Fe-O = 1.995 Å. Iron is confirmed to have square-planar coordination, and refined atomic coordinates closely agree with those determined by Pabst (1943). Maximum directions of anisotropic thermal vibrations are correlated with weakest bonding directions for all atoms in the asymmetric unit.

The unit-cell, space group, and crystal structure of gillespite II were determined at a pressure slightly above 26 kbar from three-dimensional X-ray diffraction data obtained from a single crystal mounted in a miniature high-pressure diamond cell. Gillespite II is orthorhombic $P2_12_12$ with $a = 7.349(5)$, $b = 7.515(6)$, $c = 7.894(20)$ Å, $Z = 2$, and represents a 4.0 percent volume decrease from the low pressure phase. Average bond lengths are: Si-O = 1.60, Ba-O = 2.795, and Fe-O = 1.980 Å. The iron coordination polyhedron in this high pressure phase is a distorted square plane with O-Fe-O angles of 167°. This distortion from square planar coordination is believed sufficient to explain changes in polarized absorption and Mössbauer spectra between 1 atm and 26 kbar (Hazen and Abu-Eid, 1974).

Introduction

Gillespite, $BaFeSi_4O_{10}$, was first described by Schaller (1922), who later described it as tetragonal on the basis of optical properties and cleavage (Schaller, 1929). Pabst (1943) presented the first X-ray diffraction data on gillespite, and determined the mineral's unit-cell dimensions, space group, and approximate atomic coordinates.

Gillespite is a layer silicate with four-member rings of SiO_4^{4-} tetrahedra forming the basic building blocks (Fig. 1). All apical oxygens of a given ring point in the same direction, and each ring is linked to four others with apices pointing in the opposite direction. In this way an infinite silicate tetrahedral layer with thickness equal to the height of two tetrahedra is constructed. All tetrahedra are crystallographically equivalent; within each tetrahedron are two oxygens (O2) that link tetrahedra in the same ring, one oxygen (O1) that links adjacent rings, and one non-linking oxygen (O3). Ferrous iron atoms lie on four-fold axes, and are bonded to four O3 oxygens in square-planar coordination. Interlayer barium atoms occupy $\bar{4}$ sites, and possess irregular eight coordination corresponding to a distorted cube. The fundamental inter-layer repeat (parallel to c) is 8 Å. However, the four-membered rings of silicate tetrahedra in adjacent layers are rotated approximately 15° with respect to each other; hence the true identity period parallel to c is 16 Å (Fig. 1).

The unusual square planar coordination of high-spin ferrous iron has made gillespite an interesting mineral for optical absorption and Mössbauer spectroscopic studies. Strens (1966) recorded the optical absorption spectra of gillespite at room and elevated pressures, and noted a reversible transition from the red low-pressure phase to a "colorless" high-pressure phase. Because the high-pressure spectra are relatively featureless, Strens interpreted the transition as one from high-spin to low-spin ferrous iron. An alternative hypothesis was offered by Abu-Eid, Mao, and Burns (1973) who measured polarized optical absorption spectra of gillespite at high pressures. While the authors confirmed the reversible phase transformation at a pressure of 26 ± 1 kbar, they

[1] Mineralogical contribution No. 497, Harvard University.

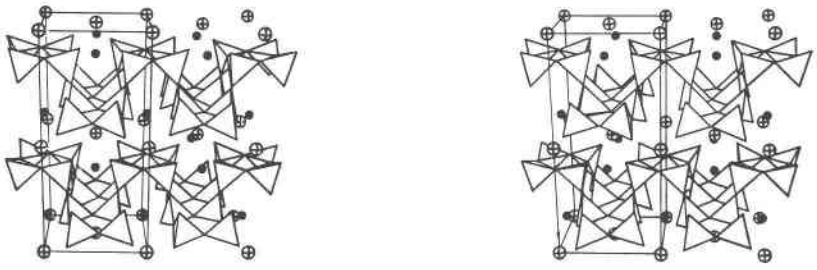

FIG. 1. Stereoscopic view of the gillespite I crystal structure. The c axis is vertical, and one unit cell is outlined. Note the two-layer repeat parallel to c; adjacent layers differ only in the relative rotation of four-member silicate rings.

observed a distinct blue color in the high-pressure phase, and a corresponding change in the high-pressure spectra. This change was attributed to a distortion of the ferrous iron coordination polyhedron from square planar to a flattened tetrahedron. High pressure Mössbauer studies were cited by Abu-Eid *et al* (1973) as further evidence favoring a coordination change rather than a change in ferrous iron spin-state.

The purpose of the present investigation was to obtain precise structural parameters for the low-pressure gillespite phase, and to determine the structure of the high-pressure phase. It was believed that comparison of these two structures would reveal the nature of the high-pressure transition and thus the cause of spectra changes between low and high pressures. Significant shortening of the Fe-O3 bonds would be expected in a high-spin to low-spin transition, while constant bond distances and changing O3-Fe-O3 angles would define a change in the ferrous iron coordination polyhedra. A secondary goal of this study was to determine the feasibility of making X-ray intensity measurements with an automated single-crystal diffractometer on a crystal held at high pressure in the miniature single crystal diamond cell.

Experimental

Specimen Description

A specimen of gillespite from the Harvard University Mineralogical Collection (HU #107555) was generously provided by Professor Clifford Frondel. Fragments of gillespite were chipped from a large plate 5 × 5 × 1 cm. This specimen has a deep red color and displays excellent basal (001) and poor (100) cleavages. Optical properties of this specimen from Esquire Mine #7, Fresno County, California, closely match those of the first-described material (Schaller, 1929) with $\epsilon = 1.620(2)$ (red) and $\omega = 1.620(2)$ (pale red). Flame photometry by Dr. Jun Ito of Harvard University confirmed that the major cations were Ba, Fe, and Si. Minor amounts of Mg, Mn, Al, and Ca, and traces of Cr, V, Sr, Cu, and Ag were also detected. Titanium was observed to be the only important minor element, and subsequent colorimetic analysis revealed 0.2 weight percent TiO_2.

Low-Pressure X-ray Diffraction and Structure Analysis

The sample was partially crushed and a rectangular cleavage plate 220 × 270 × 110 μ was selected for X-ray diffraction study. The diffraction symbol determined by Pabst (1943) was confirmed using precession photographs as $4/mmm\ P\ ncc$, which unambiguously defines space group $P4/n\,2_1/c\,2/c$. Unit-cell parameters were determined by least-squares refinement of twelve oriented reflections on our four-circle computer-controlled Picker diffractometer using procedures described by Busing and Levy (1967) and modified by Grove and Hazen (1974). The tetragonal unit-cell has $a = 7.5164(6)$ and $c = 16.0768(10)$ Å resulting in a calculated density, $\rho_{calc} = 3.404$ gm/cm^3.

Intensity measurements were performed with a four-circle computer-controlled Picker diffractometer using procedures described by Burnham *et al* (1971). All non-equivalent diffractions (*i.e.*, $h \geq k$) in one octant of reciprocal space within the range 0.09 to 0.91 sin θ/λ were measured; of the 1608 measurements, 290 were confirmed to obey space group absence criteria, and the remaining 1318 were used

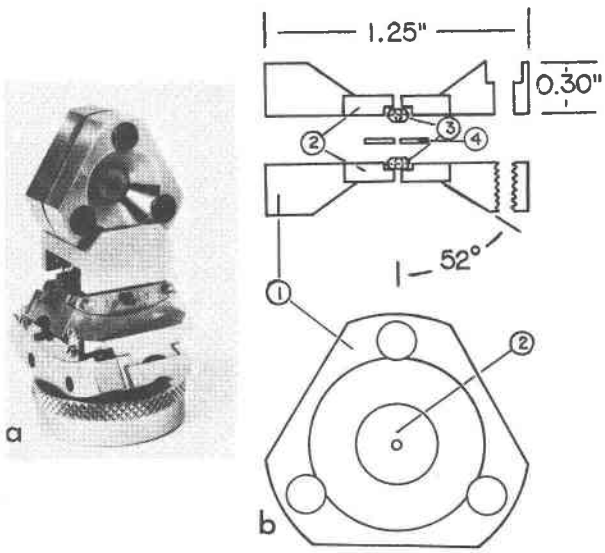

FIG. 2. (a) The Bassett miniature diamond pressure-cell mounted on a modified eucentric goniometer head. (b) Schematic diagram of the miniature gasketed diamond anvil pressure cell (from Merrill, 1973). (1) stainless steel plattens, (2) beryllium disks, (3) diamond anvils, and (4) inconel gasket.

in structure refinement.[2] Integrated intensities were corrected for Lorentz and polarization effects, and absorption corrections were computed by numerical integration (Burnham, 1966). Transmission factors for room pressure gillespite varied from 0.31 to 0.51.

Structure refinement was carried out using the full-matrix least-squares refinement program REFINE (Finger, 1969), with a weighting scheme based on counting statistics and with atomic scattering factors as described by Burnham *et al* (1971). Gillespite refinement was initialized using the atomic coordinates suggested by Pabst (1943), and after eight cycles of isotropic model refinement ($R = 4.8\%$) convergence was obtained using 1311 of the 1318 non-extinct diffractions. Seven of the ten strongest intensity measurements were rejected due to large negative values of $|F_{obs}| - |F_{calc}|$ which indicated the likelihood of significant secondary extinction effects; no further extinction correction was applied. After four additional least-squares cycles using anisotropic temperature factors for each atom, final convergence was achieved at $R = 3.3$ percent. The Fourier difference synthesis at this stage was essentially featureless.

High-Pressure X-ray Diffraction

A second rectangular single crystal plate 320 × 320 × 140 μ was selected for high-pressure X-ray diffraction study. This crystal was mounted in a miniature single-crystal high-pressure diamond cell (Merrill and Bassett, 1974; Fig. 2) using a 1.560 index-of-refraction oil as a hydrostatic pressure medium. The crystal was oriented with its c axis perpendicular to the diamond crystal faces (*i.e.*, with the basal cleavage parallel to the diamond crystals). The pressure cell was tightened slowly, by turning each of the three large screws successively in five degree increments, until a sudden red-to-blue color change was observed. The color change was uniform, rapid, and affected all portions of the crystal plate simultaneously, indicating that hydrostatic pressure of slightly above 26 kbar (the pressure of transition) had been achieved.

The miniature pressure cell was mounted on a modified eucentric goniometer head, and the unit cell and space group of the high pressure phase were determined from precession photographs. The c axis cone-axis photographs show that the c axis of high pressure gillespite (gillespite II) is approximately half that of the low pressure phase (gillespite I) (Fig. 3). Thus, the c-axis repeat of gillespite II implies a single silicate tetrahedral layer repeat (8 Å) as opposed to the double layer superstructure of gillespite I (16 Å). From c-axis precession photographs there is little change in the a dimension be-

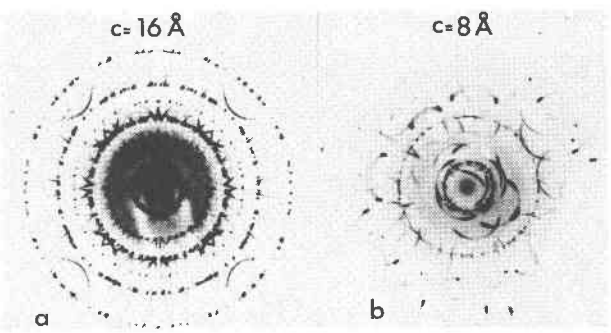

FIG. 3. c cone-axis photographs: (a) Gillespite I at 1 atm, showing 16 Å (two-layer) repeat. (b) Gillespite II at ≈26 kbar, showing 8 Å (one-layer) repeat.

[2] Tabulated observed and calculated structure factors for gillespite I and II may be obtained by ordering NAPS Document 02458 from ASIS, c/o Microfiche Publications, 305 East 46th Street, New York, N. Y. 10017. Please remit in advance $1.50 for microfiche or $5.00 for photocopies (57 pages). Please check the most recent issue of this journal for the current address and prices.

tween low and high pressure phases (Fig. 4). However, systematic extinction criteria for the *n*- and the *c*-glide planes present in gillespite I are violated by gillespite II. Reflections of the classes *h*00 and 0*l*0 with $h + k = 2n + 1$ are extinct, confirming the continued presence of 2_1 screw axes parallel to the *a* and *b* axes. The distribution of diffraction intensity appeared to conform to tetragonal symmetry; hence an initial interpretation of the precession photographs yielded diffraction symbol $4/mmm\ P\ -2_1-$ (Hazen and Abu-Eid, 1974). However, careful re-examination of intensity distributions subsequently revealed violations of 4-fold symmetry; thus the correct diffraction symbol is $mmm\ P\ 2_12_1-$. These diffraction data lead unambiguously to orthorhombic space group $P2_12_12$.

Unit-cell dimensions were determined using procedures identical to those for gillespite I, and resulting values are $a = 7.349 \pm 0.005$, $b = 7.515 \pm 0.006$, and $c = 7.894 \pm 0.020$ Å. The resulting calculated density, $\rho_{calc} = 3.546$ gm/cm^3 at approximately 26 kbar, represents a 4.00 percent decrease in volume from gillespite I. Estimated standard deviations (*esd*) for gillespite II are significantly higher than those for the low pressure phase due to increased peak width at high pressure, and corresponding errors in peak centering. Furthermore, the high *esd* of the *c* dimension of gillespite II is in part due to the mechanical limits imposed by the high-pressure cell which prevented peak centering and data collection of diffractions with $l > 3$.

Intensity measurements for gillespite II were made as described above for gillespite I. Of the 668 total diffractions accessible within the mechanical limits of the system, only 177 were non-redundant, representing 69 in class *hk*0, 67 in class *hk*1, and 41 in class *hk*2. This non-uniform sampling of reciprocal space includes values of sin θ/λ from 0.07 to 0.65, and transmission factors of 0.34 to 0.38. No corrections were made for absorption by the diamond and beryllium components of the pressure cell.

Gillespite II Structure Determination

Equipoint analysis of gillespite II ($BaFeSi_4O_{10}$, $Z = 2$, $P2_12_12$) showed that Ba and Fe occupy special postions 2*a* or 2*b* on the two-fold rotation axes parallel to *c* at (0,0,*z*) or (0,1/2,*z*) respectively. Assuming that the heavy cations of gillespite II occupy positions analogous to those of the low-pressure phase, Ba and Fe fill sites 2*a* and 2*b* respectively. All other atoms—including two silicons and five oxygens—occupy general positions. The three-dimensional Patterson function, generated using the 177 independent $|F_{obs}|^2$, exhibited strong peaks corresponding to Ba-Ba, Ba-Fe, and Fe-Fe interatomic vectors. Analysis of these peaks yielded Ba and Fe positions at (0,0,0) and (0,1/2,0.18) respectively.

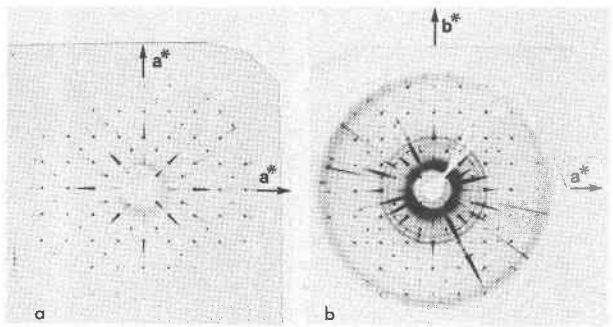

FIG. 4. *c*-axis O-level precession photographs: (**a**) Gillespite I showing $h + k = 2n + 1$ extinct. (**b**) Gillespite II at $P \approx 26$ kbar, with $h + k = 2n + 1$ present. Note streaking and powder rings due to diffraction from diamond and beryllium components of the miniature pressure cell.

Although gillespite II is noncentrosymmetric, we proceeded with our analysis under the assumption that its structure is likely to be simply a distortion of that of low pressure gillespite, which is centrosymmetric. Presumably the rapid and reversible transformation from I to II is displacive and involves only small departures from inversion symmetry; thus all structure-factor phase angles for gillespite II should be reasonably close to 0 or π, provided the origin is properly chosen. To take advantage of this simplifying assumption, a non-standard origin for the orthorhombic cell was selected at (1/4,-1/4,0), corresponding to the position of an inversion center in the low pressure structure referred to the standard setting in supergroup $P4/ncc$. With this origin shift, the coordinates of barium and iron become (1/4, 3/4,0) and (1/4,1/4,0.18) respectively.

Observed structure factors were scaled using Wilson statistics (Lipson and Cochran, 1966; Hanscom, 1973) and were then compared with those calculated for a model with only barium and iron atoms. Diffractions for which 50 percent or less of the maximum scattering from eight silicons plus twenty oxygens with unknown coordinates could not change the calculated sign—*i.e.*, for a given sin θ/λ: $1/2(8f_{Si} + 20f_O) < F_{obs} + |A_{calc}|$—were separated, and these 72 structure factors with signs assumed to to have been fixed by Ba and Fe contributions were

TABLE 1. Atomic Coordinates and Thermal Parameters

Atom	x	y	z	β_{11}[a]	β_{22}	β_{33}	β_{12}	β_{13}	β_{23}	B_{equiv}[b]
Gillespite I (P = 1 atm)										
Ba	0	0	0	0.00435(4)[c]	0.00435(4)	0.00062(1)	0	0	0	0.87(1)
Fe	0	1/2	0.0920(1)	0.00199(8)	0.00199(8)	0.00126(3)	0	0	0	0.74(1)
Si	0.2691(1)	0.1854(1)	0.1548(1)	0.00198(15)	0.00180(14)	0.00085(3)	-.0000(1)	0.0002(1)	-.0002(1)	0.58(1)
O1	0.2242(4)	0.2242(4)	1/4	0.0116(6)	0.0116(6)	0.00169(12)	-.0037(7)	0.0020(3)	-.0020(3)	2.33(5)
O2	0.4723(4)	0.2475(4)	0.1377(1)	0.0026(5)	0.0093(5)	0.00141(8)	-.0006(3)	-.0002(2)	0.0011(2)	1.38(5)
O3	0.1415(4)	0.2754(4)	0.0900(2)	0.0056(5)	0.0019(5)	0.00306(13)	0.0020(4)	-.0021(2)	-.0007(2)	1.62(6)
Gillespite II (P = 26 kbar)				B (Å^2)						
Ba	0	0	0.000(3)	3.0(2)						
Fe	0	1/2	0.185(4)	1.6(4)						
SiA	0.680(4)	0.215(3)	0.330(5)	1.5(6)						
SiB	0.270(3)	0.190(3)	0.290(7)	1.4(6)						
O1	0.255(5)	0.265(4)	0.48(1)	5.0(2.0)						
O2A	0.480(4)	0.215(5)	0.245(10)	2.9(1.7)						
O2B	0.245(5)	0.978(4)	0.28(1)	13.3(2.3)						
O3A	0.230(6)	0.635(5)	0.21(1)	12.1(2.7)						
O3B	0.145(6)	0.280(5)	0.155(10)	1.9(1.4)						

a) The anisotropic temperature factor form is $\exp[-\Sigma_i\Sigma_j\beta_{ij}h_ih_j]$.

b) Equivalent isotropic temperature factors are computed according to $B_{equiv.} = 4/3\ \{\Sigma_i\Sigma_j\beta_{ij}a_i\cdot a_j\}$, and are related in the standard way to a vibration sphere that approximates the vibration ellipsoid described by the anisotropic temperature factor tensor (Hamilton, 1959).

c) Parenthesized figures represent the estimated standard deviation (esd) in terms of least units cited for the value to the immediate left, thus 0.00435(4) indicates an esd of 0.00004.

used to generate a three-dimensional Fourier synthesis of the electron density. Analysis of the electron density plot revealed, as expected, sharp maxima at the positions of Ba and Fe, as well as additional maxima near locations analogous to gillespite I silicon positions. However, the positive electron density in regions near expected oxygen positions was too diffuse to allow us to resolve these anion locations.

The above procedure was repeated, with observed structure factors being compared to those calculated for a model containing Ba, Fe, Si*A*, and Si*B*. The 114 structure factors having known signs were used to generate a second three-dimensional Fourier synthesis, and in this plot electron density maxima were found corresponding to all atoms. While x and y coordinates of all atoms were well-defined, z coordinates of the five oxygen atoms in the asymmetric unit were difficult to evaluate due to diffuseness of electron density parallel to [001].

Using atomic coordinates determined from the Fourier map, and isotropic temperature factors of gillespite I, an attempt was made to refine the atom parameters of gillespite II by least-square methods. While values of x and y for all atoms, and z for all cations, converged, the five oxygen z coordinates did not. This was not surprising considering that (1) minimal c-axis data was available since all reflections had $l \leq 2$; (2) only 177 observations were used in the refinement and of these only 134 $|F_{obs}|$ had values above the minimum observable; and, finally, (3) no account was taken of absorption by diamond and beryllium of the pressure cell and errors in absorption corrections could thus exceed 10 percent.

An alternate approach to determine the five unknown oxygen z coordinates was to assume that Si-O bond distances are approximately 1.60 Å, and that tetrahedral O-O bond distances exceed 2.45 Å. These values for bond distances are consistent with known linear compressibilities of quartz at 30 kbar (Clark, 1966). Given these assumptions and the known cation positions, a unique set of z coordinates was found. Values were rounded off to the nearest 0.005 fractional unit, and estimated standard deviations of 0.01 were assumed for z coordinates of these five oxygen atoms. Comparison of the resulting model with observed structure factors gave the lowest R for any gillespite II model: $R = 10.5$ percent. However, attempts to refine isotropic temperature factors for all atoms in this model were unsuccessful because of the extreme diffuseness of electron density in the regions about the oxygen positions.

Unrealistic temperature factors exceeding 10.0 Å² were obtained for four of the five oxygens in the asymmetric unit.

Discussion

Gillespite I

Atomic coordinates and anisotropic temperature factors for gillespite I are presented in Table 1, while principal bond distances and bond angles appear in Table 2. Refined values of atomic coordinates agree closely with those of Pabst (1943), and in no instance deviate by more than 0.01 fractional units from the 1943 determination.

As determined by Pabst, the iron and O3 oxygens depart only 0.03 Å from being coplanar. Thus the iron atoms in sites with point symmetry 4 have a first coordination close to an ideal square planar configuration (Fig. 5a). The observed Fe-O3 bond distance of 1.995 Å is similar to the 2.020 Å value determined by Smith (1968) for a tetrahedral site in staurolite having approximate occupancy of $(Fe^{2+}_{0.64}Al_{0.32}Ti_{0.04})$.

The silicate tetrahedron has a mean Si-O distance of 1.603 Å, which is close to the 1.608 Å value observed for pure silicate mica-like tetrahedral layers (Hazen and Burnham, 1973). The Si-O3 bond is unusually short (1.569 Å), very likely because of the charge undersaturation of O3, which is bonded to one $Fe^{(2+)IV}$, one Ba^{VIII}, and one Si^{IV}. On the other hand, the two Si-O2 bonds (1.620 and 1.630 Å) are longer than the average due to charge oversaturation of O2, which is bonded to two Si^{IV} and one Ba^{VIII}. The Si-O1 bond distance (1.594 Å) is closest to the average (1.604 Å) as expected since O1 is saturated by two silicon atoms. The O-Si-O bond angles deviate as much as six degrees from the ideal 109.47° for a regular tetrahedron. The angles O3-Si-O1 (105.4°) and O3-Si-O2 (115.4°) show, by far, the greatest deviation from the ideal, and may once again be interpreted as a result of distortions due to the undersaturation of O3.

The bond distances and angles of the silicate tetrahedral layer in gillespite I are also consistent with predictions made by *d-p* π-bonding theory

TABLE 2. Interatomic Distances and Bond Angles

Bond	Distance (Å)	Atoms	Angle (°)	Bond	Distance (Å)	Atoms	Angle (°)
Gillespite I				Gillespite II			
Si-O1	1.594(1)[1]	O1-Si-O2	108.1(2)	SiA-O1	1.60(1)	O1-SiA-O2A	118(5)
Si-O2	1.620(3)	O1-Si-O2	109.0(2)	SiA-O2A	1.62(1)	O1-SiA-O2B	101(4)
Si-O2	1.630(3)	O1-Si-O3	115.4(1)	SiA-O2B	1.60(1)	O1-SiA-O3A	110(4)
Si-O3	1.569(3)	O2-Si-O2	109.1(2)	SiA-O3A	1.61(1)	O2A-SiA-O2B	102(3)
Mean Si-O	1.603	O2-Si-O3	105.4(1)			O2A-SiA-O3A	99(3)
		O2-Si-O3	109.8(2)			O2B-SiA-O3A	110(4)
Si-Si	3.188(2)	Si-O1-Si	177.7(3)	SiB-O1	1.60(1)	O1-SiB-O2A	104(4)
Si-Si [2][2]	3.147(2)	Si-O2-Si	151.2(2)	SiB-O2A	1.57(2)	O1-SiB-O2B	113(4)
				SiB-O2B	1.59(1)	O1-SiB-O3B	116(4)
				SiB-O3B	1.61(1)	O2A-SiB-O3B	103(3)
						O2A-SiB-O3B	111(4)
						O2B-SiB-O3B	109(4)
				SiA-SiB	3.16(3)	SiA-O1-SiB	158(3)
				SiA-SiB	2.91(3)	SiA-O2A-SiB	142(6)
				SiA-SiB	2.89(3)	SiA-O2B-SiB	148(4)
Fe-O3 [4]	1.995(3)	O3-Fe-O3	178.2(2)	Fe-O3A [2]	1.98(3)	O3A-Fe-O3A	168(5)
		O3-Fe-O3	90	Fe-O3A [2]	1.98(3)	O3A-Fe-O3B	89(2)
						O3A-Fe-O3B	92(2)
						O3B-Fe-O3B	166(5)
Ba-O2 [4]	2.923(3)			Ba-O2A [2]	2.89(5)		
Ba-O3 [4]	2.741(3)			Ba-O2B [2]	2.86(5)		
				Ba-O3A [2]	2.78(5)		
				Ba-O3B [2]	2.66(5)		

1. Parenthesized figures represent the estimated standard deviation (esd) in terms of least units cited for the value to the immediate left, thus 1.594(1) indicates an esd of 0.001.
2. Bracketed figures represent multiplicity of the bond to the immediate left.

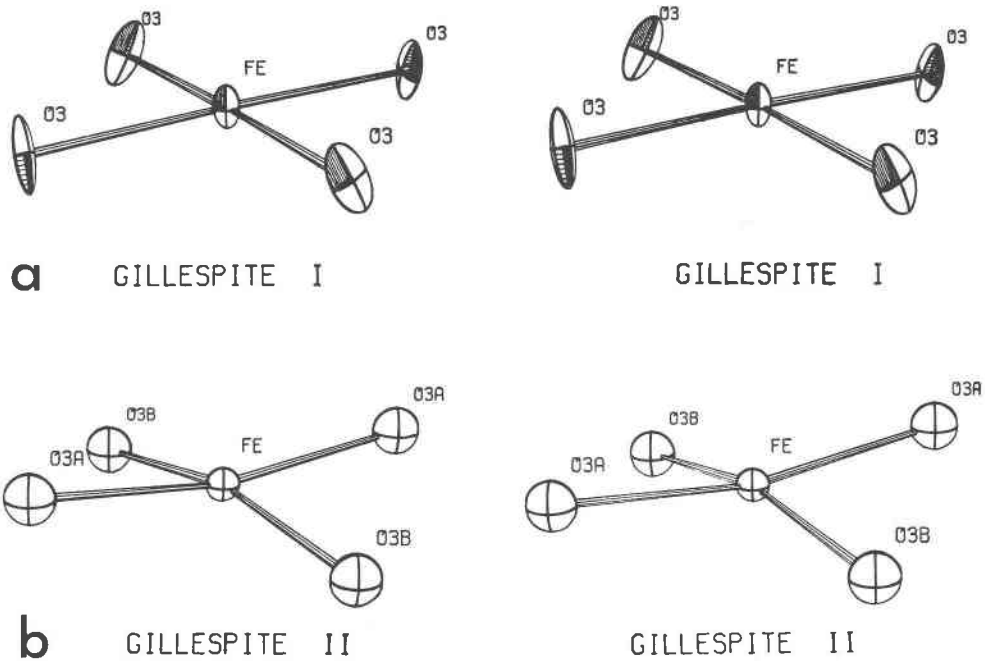

FIG. 5. Stereoscopic view of the iron coordination polyhedra. (**a**) Gillespite I iron, square planar coordination with Fe-O = 1.995 Å and O-Fe-O = 178°. Ellipsoids represent 50 percent probability distribution of anisotropic thermal motion. (**b**) Gillespite II iron, distorted square planar coordination with Fe-O = 1.98 Å and O-Fe-O = 167°. Thermal motion is assumed to be isotropic.

(Brown and Gibbs, 1970). As expected, the bond from Si to the one non-bridging (nbr) oxygen O3 is shorter than the other three silicon bonds with bridging (br) oxygens O1 and O2. Thus, the variation of silicon-oxygen bond lengths may be explained by a combination of π-bonding and electrostatic effects. Also as predicted, the shortest Si-O_{br} bonds are associated with the largest Si-O-Si bond angles: Si-O1-Si = 177.7° and Si-O1 = 1.594 Å, while Si-O2-Si = 151° and Si-O2 = 1.620 and 1.630 Å. Finally, the average O_{nbr}-Si-O_{br} bond angle (110.2°) is greater than the average O_{br}-Si-O_{br} bond angle (108.7°).

Louisnathan and Gibbs (1972) have used extended Hückel molecular orbital calculations to demonstrate that for the average of the O-Si-O angles ($\langle$O-Si-O$\rangle_3$) common to each Si-O bond, as the $\langle$O-Si-O$\rangle_3$ angle increases in value, the bond common to these three angles decreases in length. This prediction is generally true for gillespite I with $\langle$O1-Si-O$\rangle_3$ = 111.8°, d(Si-O1) = 1.594 Å; $\langle$O3-Si-O$\rangle_3$ = 110.2°, d(Si-O3) = 1.569 Å; $\langle$O2-Si-O$\rangle_3$ = 108.7°, d(Si-O2) = 1.620 Å; and $\langle$O2-Si-O$\rangle_3$ = 108.1°, d(Si-O2) = 1.630 Å. Hence wider values of $\langle$O-Si-O$\rangle_3$ are associated with shorter Si-O bond lengths.

An unusual aspect of the gillespite I structure is the Si-O1-Si bond angle which represents the linking of adjacent rings of tetrahedra (Fig. 6). While Si-O-Si bond angles are usually around 145° ± 15°, the Si-O1-Si angle of 177.7° indicates a near maximum separation between adjacent rings. Liebau (1961) stated that under normal conditions Si-O-Si angles greater than 160° do not exist in crystalline silicates, and he discounted previous structure determinations of thortveitite ($Sc_2Si_2O_7$), coesite (SiO_2), and gillespite for which 180° Si-O-Si bond angles were thought to occur. However, structure refinements of thortveitite (Smolin, Shepelov, and Titov, 1973; Prewitt, unpublished) and coesite (Araki and Zoltai, 1969; Prewitt, unpublished), as well as this study, confirm the existence of near-straight Si-O-Si bonds.

The barium, occupying a site with $\bar{4}$ symmetry, has distorted cubic eight-coordination with four Ba-O3 bonds of 2.741 Å, and four Ba-O2 bonds of 2.923 Å. As expected, the bonds from Ba to the charge-undersaturated O3 are considerably shorter than

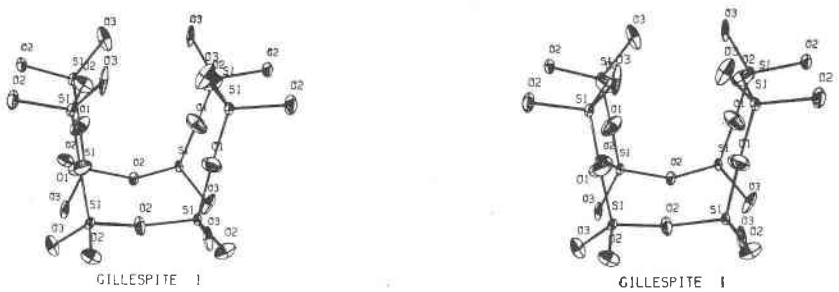

FIG. 6. Stereoscopic view of a portion of the gillespite I silicate layer. Note the near-straight (178°) Si-O1-Si bond angle.

those to the oversaturated O2 oxygens. The mean barium-oxygen bond distance is 2.832 Å.

Magnitudes and orientations of atomic thermal vibration ellipsoids are presented in Table 3, and are illustrated in Figures 1, 5a, and 6. Thermal vibrations of gillespite I anions are significantly larger than those found in many silicates (Burnham, 1965). Oxygen O1, which is coordinated to only two cations and participates in the 178° Si-O1-Si bond angle, has the largest observed thermal motion ($B_{equiv} = 2.33$), while O2 and O3 are coordinated to three cations and have isotropic temperature factors of 1.38 and 1.62 respectively. Cation thermal vibrations are somewhat larger than those of many silicates.

Maximum vibration directions can be correlated with weakest bonding directions. For example, iron shows its maximum vibration perpendicular to the (001) plane containing the four Fe-O3 bonds. Similarly, O1 has its two largest vibration directions perpendicular to the Si-O-Si bonds. Analogous vibration behavior is seen for O2 and O3. Barium and silicon, which are uniformly surrounded by oxygens, show the least anisotropic behavior in gillespite I. The anisotropy of oxygen O3 is abnormally high, with 3:1.5:1 elongation of the thermal vibration ellipsoid (Fig. 5a). This apparent vibration behavior suggested to us the possibility of a split-atom model for O3, and a fine-scale Fourier synthesis was generated for the region around this atom. The electron density map confirmed the extreme elongation of electron density, but no evidence for a double maximum was found.

Gillespite II

Atomic coordinates for gillespite II are presented in Table 1. In the apparently displacive transformation from gillespite I to II, the c axis is halved, and the space group changes from $P4/n\,2_1/c\,2/c$ to $P2_12_12$. The six atoms in the asymmetric unit of gillespite are increased to nine in this change of symmetry, with Si, O2, and O3 of the low pressure phase becoming SiA and SiB, O2A and O2B, and O3A and O3B of the high pressure phase respectively. In terms of fractional coordinates, no atoms shift more than 0.08 units, and the average shift is 0.015 fractional units (assuming $\Delta z = |z_{II} - 2 \cdot z_I|$ due to the change in c axis).

Of considerable interest to spectroscopists are the changes in coordination and bond distances of iron. In gillespite II, as in gillespite I, there are four Fe-O3 (A and B) bonds. Fe-O3 bond lengths in gillespite II

TABLE 3. Magnitudes and Orientations of Thermal Ellipsoids for Gillespite I

Atom	Axis	rms Displacement (Å)	Angle with respect to: a (°)	b (°)	c (°)
Ba	r_1	0.0899(6)[1]	90	90	0
	r_2	0.1116(3)	0	90	90
	r_3	0.1116(3)	90	0	90
Fe	r_1	0.0755(1)	0	90	90
	r_2	0.0755(1)	90	0	90
	r_3	0.1287(15)	90	90	0
Si	r_1	0.070(3)	104(30)	20(25)	76(5)
	r_2	0.074(3)	18(23)	74(30)	99(8)
	r_3	0.108(2)	78(3)	101(3)	17(3)
O1	r_1	0.112(6)	110(5)	70(4)	29(2)
	r_2	0.150(7)	135	135	90
	r_3	0.231(5)	52(2)	128(2)	61(2)
O2	r_1	0.085(9)	7(5)	87(4)	84(6)
	r_2	0.121(5)	86(7)	60(4)	150(4)
	r_3	0.174(5)	95(3)	30(4)	61(4)
O3	r_1	0.052(12)	63(5)	153(6)	87(3)
	r_2	0.109(6)	142(5)	115(6)	116(2)
	r_3	0.216(4)	114(2)	98(2)	26(2)

1. Parenthesized figures represent the estimated standard deviation (esd) in terms of least units cited for the value to the immediate left, thus 0.0899(6) indicates an esd of 0.0006.

(calculated to be 1.98 Å) are only slightly shorter than those of gillespite I (1.995 Å); thus iron is in the high-spin state in both structures. However, there is a definite change in shape of the coordination polyhedra (Fig. 5). Instead of a nearly ideal square planar configuration with O3-Fe-O3 bond angles of 178°, the gillespite II iron coordination polyhedron is essentially a distorted square-plane with angles O3*A*-Fe-O3*A* and O3*B*-Fe-O3*B* equal to 167°. Perhaps the distortion is sufficient to label the polyhedron an extremely flattened tetrahedron, but regardless of geometric preference it is probably sufficient to account for observed changes in both polarized absorption and Mössbauer spectra at high pressure (Hazen and Abu-Eid, 1974).

The tetrahedral silicate layer of gillespite II is illustrated in Figure 7. The greatest shift in coordinates from gillespite I to II occurs for O1, and the greatest change in bond angles is similarly for Si-O1-Si. The change in Si-O1-Si bond angle from 177.7° in gillespite I to 158° in gillespite II is consistent with the increased density of the high pressure phase in which silicate tetrahedra of adjacent four-member rings are more closely packed. In fact, the decrease in Si-Si distances between adjacent rings from 3.1 Å to 2.9 Å between the low and high pressure phases is sufficient to account for the decrease in the one-layer *c*-axis repeat from 8.04 Å to 7.89 Å. As mentioned previously, the *c* axis in gillespite I corresponds to a two-layer periodicity characterized by 15° relative rotation of the four-member rings in alternate layers. In gillespite II all layers are rotated in the same sense, thus destroying the double-layer repeat. A detailed analysis of the stereochemistry of gillespite II is not practical at this time, since the *z* coordinates of all oxygens are unrefineable with our present data and they were calculated assuming an Si-O bond distance of approximately 1.60 Å.

The gillespite II barium atom has 8-coordination with an oxygen polyhedron best described as a distorted rectangular antiprism. The change from distorted cubic coordination in gillespite I to the antiprism coordination of the high pressure phase is directly related to the change from a two-layer structure with opposing rotations of tetrahedral rings in adjacent layers, to the one-layer repeat of gillespite II. The Ba-O distances in high-pressure gillespite range from 2.66 to 2.89 Å, and the mean barium-oxygen distance has decreased from 2.832 to 2.795 Å through the phase transition.

Nature of the Phase Transformation

Observations of the gillespite color change and comparison of both crystal structures indicate that the phase transformation is rapid, reversible, and displacive (or distortional), assuming the color changes and the structural transformation take place simultaneously. No changes of primary coordination number of any atoms occur. While the Fe^{2+} square-planar coordination geometry distorts and the linkages between four-membered silicate tetrahedral rings become kinked, the largest distortion involves the change of the eight oxygens around Ba from a non-ideal cube with $\bar{4}$ symmetry to a distorted rectangular anti-prism with only 2-fold symmetry.

Since the transformation is characterized by structural distortions that break neither primary coordination bonds nor polyhedral linkages, it is possible that its thermodynamic behavior is not first order. Second-order character, implying a discontinuity at the transformation pressure in isothermal compressibility but not molar volume (Denbigh, 1966), would require that the symmetry of high pressure gillespite be a subgroup of that of low pressure gillespite. Although cursory comparison of the two space groups—$P4/ncc$(I) *vs* $P2_12_12$(II)—suggests

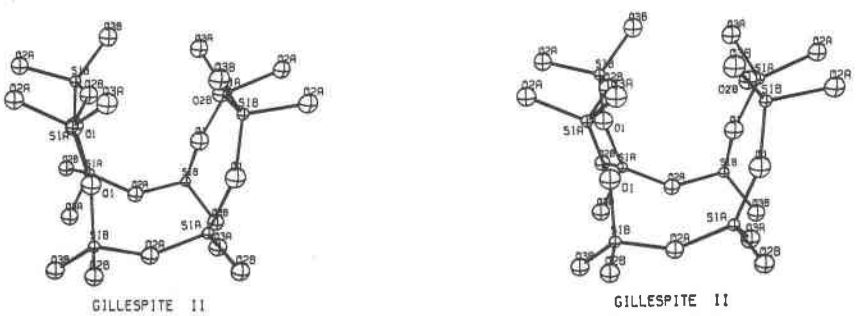

FIG. 7. Stereoscopic view of a portion of the gillespite II silicate layer. Angle Si-O1-Si is 157°. Thermal motion is assumed to be isotropic.

an appropriate subgroup relationship, the translational symmetry of gillespite II along c is 8 Å rather than 16 Å. One consequence of additional translational symmetry in the high pressure phase is a doubling in number of 2_1 axes normal to c. Thus the orthorhombic symmetry of gillespite II cannot be derived simply by suppressing some symmetry elements of tetragonal gillespite I.

One possible explanation for the unexpected symmetry relationship is that the 8 Å c-axis translation does not represent the true periodicity, and evidence for a 16 Å superstructure is obliterated by averaging over small anti-phase domains. If the pressure-induced distortions were to take place in such manner as to maintain the 2-layer 16 Å repeat in any given unit cell, but were to "nucleate" simultaneously in different layers in various regions of the crystal, distorted 16 Å-repeat domains would develop that would meet at boundaries out of step by 1/2 **c**, or 8 Å. Were such domains sufficiently small (on the order of several unit cells), diffraction would maintain coherency across domain boundaries, subcell contributions to reflections with l odd would destructively interfere, and an average 8 Å pattern would emerge. Structure analysis would yield an average atomic configuration. Although the apparent thermal vibrations in gillespite II are abnormally large and perhaps indicative of an average structure, we believe they compensate primarily for absorption effects of the pressure cell. Furthermore, the gillespite II configuration is not a likely average of configurations easily derived by distortions of the two layers of gillespite I; indeed the rotational sense of the gillespite II tetrahedral rings more closely resembles that of the rings in one gillespite I layer rather than an average of the two gillespite I rings. While it may seem inappropriate to devise a domain model only to assert its incorrectness, the analysis lends strong support to our view that the gillespite II structure is real—not an average—and that our observations reveal its true symmetry.

On the basis of the observed symmetry and structural relationships, we believe the gillespite phase transformation is structurally displacive and thermodynamically first order, but involves little or no activation energy. The changes in Ba coordination polyhedron geometry from a distorted cube to the more dense rectangular anti-prism coupled with simultaneous kinking of silicate tetrahedral linkages represent the chief structural responses to increased pressure. Slight distortion of the Fe^{2+} square-planar configuration accompanies these changes. Confirmation of our views must await structural examinations at intermediate pressures below the transition. Hysteresis effects associated with the transition are expected to be very small, and essentially impossible to observe with present equipment.

Conclusion

Until recently high-pressure single-crystal X-ray diffraction techniques were unknown. With the introduction of the Bassett miniature pressure cell, X-ray diffraction experiments at elevated pressures are now possible. The phase transformation of gillespite which occurs at 26 kbar and 23°C provides an excellent example of the types of displacive changes which may occur in silicate minerals at high pressures. In gillespite all cation coordination groups are altered at high pressures. Square-planar iron with 4-fold symmetry transforms to a distorted plane with 2-fold symmetry. Barium changes from distorted cubic coordination to a more closely-packed distorted square antiprism at high pressures. And while individual tetrahedra do not change significantly, angles between tetrahedra do alter, as evidenced by the change in Si-O1-Si angles from 178° to 157°. Future studies on other silicate minerals are certain to reveal similar striking alterations of crystal structure at elevated pressures.

Acknowledgments

The authors gratefully acknowledge the aid and advice of Professor William Bassett, who developed the miniature high-pressure diamond cell. Special thanks are also due to Professor Charles Prewitt, Professor Roger Strens, and Dr. R. D. Shannon for stimulating discussions and helpful suggestions regarding the nature of the gillespite phase transformation, and to Professor G. V. Gibbs for his critical review of the manuscript.

This research was supported by National Science Foundation grants GA-12852 and GA-41415.

References

Abu-Eid, R. M., H. K. Mao, and R. G. Burns (1973) Polarized absorption spectra of gillespite at high pressure. *Carnegie Inst. Wash. Year Book*, **72**, 564–567.

Araki, T., and T. Zoltai (1969) Refinement of a coesite structure. *Z. Kristallogr.* **129**, 381–387.

Brown, G. E., and G. V. Gibbs (1970) Stereochemistry and ordering in the tetrahedral portion of silicates. *Am. Mineral.* **55**, 1587–1607.

Burnham, C. W. (1965) Temperature parameters of silicate crystal structures (abstr.). *Am. Mineral.* **50**, 282.

——— (1966) Computation of absorption corrections and the significance of end-effect. *Am. Mineral.* **51**, 159–167.

———, Y. Ohashi, S. S. Hafner, and D. Virgo (1971)

Cation distribution and atomic thermal vibrations in an iron-rich orthopyroxene. *Am. Mineral.* **56,** 159–167.

BUSING, W. R., AND H. A. LEVY (1967) Angle calculations for 3- and 4-circle X-ray and neutron diffractometers. *Acta Crystallogr.* **A24,** 321–324.

CLARK, S. P., Ed. (1966) *Handbook of Physical Constants. Geol. Soc. Am. Mem.* **97,** New York, N.Y., 587 p.

DENBIGH, K. (1966) *The Principles of Chemical Equilibrium.* Cambridge, Cambridge University Press, 494 p.

FINGER, L. (1969) Determination of cation distribution by least-squares refinement of single-crystal X-ray data. *Carnegie Inst. Wash. Year Book,* **67,** 216–217.

GROVE, T. L., AND R. M. HAZEN (1974) Alkali feldspar unit cell parameters at liquid nitrogen temperature: low temperature limits of the displacive transformation. *Am. Mineral.* **59,** 1327–1329.

HAMILTON, W. C. (1959) On the isotropic temperature factor equivalent to a given anisotropic temperature factor. *Acta Crystallogr.* **12,** 609–610.

HANSCOM, R. H. (1973) *The Crystal Chemistry and Polymorphism of Chloritoid.* Ph.D. Thesis, Harvard University, Cambridge, Massachusetts.

HAZEN, R. M., AND R. M. ABU-EID (1974) Crystallography of the displacive high pressure gillespite phase transformation (abstr.). *Trans. Am. Geophys. Union,* **55,** 463.

HAZEN, R. M., AND C. W. BURNHAM (1973) The crystal structures of one-layer phlogopite and annite. *Am. Mineral.* **58,** 889–900.

LIEBAU, F. (1961) Untersuchungen über die grösse des Si-O-Si-valenzwinkels. *Acta Crystallogr.* **14,** 1103–1109.

LIPSON, H., AND W. COCHRAN (1966) *The Determination of Crystal Structures.* Cornell Univ. Press, Ithaca, New York, 414 p.

LOUISNATHAN, S. J., AND G. V. GIBBS (1972) Bond length variation in TO_4^{n-} tetrahedral oxyanions of the third row elements: T = Al,Si,P,S and Cl. *Materials Res. Bull.* **7,** 1281–1292.

MERRILL, L. (1973) *Crystallographic Studies of the Metastable High Pressure Phases of Calcium Carbonate, $CaCO_3$(II) and $CaCO_3$(III).* Ph.D. Thesis, University of Rochester, Rochester, New York, 78 p.

———, AND W. A. BASSETT (1974) Miniature diamond anvil pressure cell for single crystal X-ray diffraction studies. *Rev. Sci. Instrum.* **45,** 290–294.

PABST, A. (1943) Crystal structure of gillespite, $BaFeSi_4O_{10}$. *Am. Mineral.* **28,** 372–390.

SCHALLER, W. T. (1922) Gillespite, a new mineral. *J. Wash. Acad. Sci.* **12,** 7–8.

——— (1929) The properties and associated minerals of gillespite. *Am. Mineral.* **14,** 319–322.

SMITH, J. V. (1968) The crystal structure of staurolite. *Am. Mineral.* **53,** 1139–1155.

SMOLIN, Y. I., Y. F. SHEPELOV, AND A. P. TITOV (1973) Refinement of the crystal structure of thortveitite $Sc_2Si_2O_7$. *Sov. Phys. Crystallogr.* **17,** 749–750 (English ed.).

STRENS, R. G. J. (1966) Pressure-induced spin-pairing in gillespite, $BaFe(II)Si_4O_{10}$. *Chem. Commun.* **21,** 777–778.

Manuscript received, May 27, 1974; accepted for publication, July 18, 1974.